Correction of Nonuniform Attenuation in Cardiac SPECT Imaging

Benjamin M. W. Tsui, Grant T. Gullberg, Eric R. Edgerton, J. Glen Ballard,
J. Randolph Perry, William H. McCartney, and Jan Berg

Department of Radiology, The University of North Carolina at Chapel Hill,
Chapel Hill, North Carolina; Department of Radiology, The University of Utah, Salt Lake City
Utah; and General Electric Medical System Groups, Milwaukee, Wisconsin

Correction for photon attenuation in cardiac SPECT imaging using a measured attenuation distribution with an iterative expectation maximization (EM) algorithm and an iterative Chang algorithm were compared with the conventional filtered backprojection and an iterative EM algorithm without attenuation correction. The attenuation distribution was determined from a transmission computed tomography study that was obtained using an external collimated sheet source. The attenuation of the emitting photons was modeled in the EM algorithm by an attenuated projector-backprojector that used the estimated attenuation distribution to calculate attenuation factors for each pixel along each projection and backprojection ray. Results from a heart-lung phantom study and a ^{201}Tl patient study demonstrated that the iterative EM algorithm with attenuation correction provided improved image quality in terms of reduced streak artifacts and noise, and more accurate quantitative information in terms of improved radioactivity distribution uniformity where uniformity existed, and better anatomic object definition.

While single photon emission computed tomography (SPECT) imaging has become a routine clinical procedure in nuclear medicine, the problem of photon attenuation compensation persists for nonuniform distributions of attenuation coefficients. Most conventional attenuation correction methods in SPECT attempt to correct for photon attenuation by assuming a constant attenuation coefficient distribution. For the chest cardiac region, which contains tissues with markedly different attenuation coefficients, these methods prove to be totally inadequate. In this paper we show that the image quality and the quantitative information in cardiac SPECT imaging is improved by reconstructing the emission distribution with an iterative reconstruction algorithm that uses a measurement of the nonuniform attenuation distribution to more accurately model the attenuation of the internal emitting photons. It is recognized that the necessity to use iterative algorithms and the requirement to measure the attenuation distribution has slowed the advancement

of cardiac SPECT imaging. However, it is felt that quantitative cardiac imaging can become a reality in clinical nuclear medicine through improved digital processors and camera hardware.

Iterative algorithms are required to solve the attenuation problem for variable attenuation distributions since an analytic solution to the inverse attenuated Radon transform does not exist (*1*). However, because of the extensive computation time that iterative algorithms require, approximate and more efficient solutions have been pursued. The Chang algorithm (*2*) was originally implemented as a multiplicative postprocessing attenuation correction method to correct for photon attenuation in a uniform attenuator. This method was later applied to the variable attenuation problem using the correct nonuniform attenuation distribution to determine for each pixel a multiplicative factor that is equal to the average attenuation over all angles sampled (*3,4*). It was found that this approach could give a better solution by applying one or more iterations (*3,4*) and, thus, was termed the iterative Chang algorithm. We show that a more accurate solution to the nonuniform attenuation problem in cardiac SPECT imaging is obtained using an iterative algorithm with a projector-backprojector that models the attenuation of photons

along projection and backprojection rays and that calculates attenuation factors for each pixel along each ray from the predetermined attenuation distribution (5). The attenuated projector-backprojector models the system of projection equations which can be solved using iterative reconstruction algorithms such as the algebraic reconstruction technique (ART) (6), conjugate gradient (7), expectation maximization (EM) (8,9), and maximum entropy method (10,11,12).

An estimate of the variable attenuation distribution does not require high contrast resolution because the precision in cardiac SPECT is dominated by the emission statistics, but requires accurate delineation of the boundaries separating the lung and soft-tissue regions. Since these regions vary significantly from patient to patient, they can only be accurately specified by a transmission CT study. A few studies have previously been performed to evaluate the potential for using a transmission CT study to correct for attenuation in the chest region. An early cardiac study with ^{201}Tl used transmission data and an iterative conjugate gradient algorithm to correct for attenuation (13). More recently, clinical evaluation of this approach to correct for attenuation in liver studies was performed using transmission data and a maximum likelihood, iterative EM algorithm (14). While these studies demonstrated qualitatively the potential of accurate attenuation correction, they did not give a quantitative evaluation by means of phantom studies.

In this study we evaluated attenuation correction with both a phantom and a patient study using an external collimated flood source to determine the attenuation distribution. Four reconstruction algorithms were evaluated: filtered backprojection without attenuation correction, iterative EM without attenuation correction, iterative Chang with attenuation correction, and iterative EM with attenuation correction. The results of a phantom study and a stress ^{201}Tl patient study using these four reconstruction algorithms were evaluated for image quality and for uniformity of reconstruction across regions of equal concentration. Evaluations were made to determine if the results of the patient study correlated with those of the phantom study.

THEORY

Attenuated Projector-Backprojector for Iterative Reconstruction Algorithms

In iterative reconstruction algorithms for SPECT, a new estimate of the radioactivity distribution is obtained during each iteration using one projection and one backprojection operation. Attenuation correction can be incorporated into the reconstruction algorithm during these operations based upon a priori knowledge of the attenuation coefficient distribution. A ray-driven projector-backprojector which incorporates the attenuation correction was derived (5). As shown for

the ray in Figure 1, the projection data at bin k and angle θ_m is given by

$$p_{km} = \sum_{i,j} W_{ij}(k, m)x_{ij}, \qquad (1)$$

where x_{ij} is the image value at pixel (i,j) and $W_{ij}(k,m)$ is the probability of detection at projection bin k and angle θ_m given that the pixel (i,j) is within the detected solid angle. The weighting factor $W_{ij}(k,m)$ is given by

$$W_{ij}(k, m) = \begin{cases} \dfrac{A_{ij}(k, m)}{\mu_{ij}} \{1 - \exp[-\mu_{ij}l_{ij}(k, m)]\}, \\ \qquad\qquad\qquad\qquad\qquad\text{if } \mu_{ij} > 0 \\ l_{ij}(k, m) A_{ij}(k, m), \\ \qquad\qquad\qquad\qquad\qquad\text{if } \mu_{ij} = 0 \end{cases} \qquad (2)$$

where μ_{ij} is the attenuation coefficient of pixel (i,j) and $l_{ij}(k,m)$ is the ray length within pixel (i,j) for bin k and angle θ_m. The attenuation factor $A_{ij}(k,m)$ is the exponential of the line integral of the attenuation from the point b_{ij} (Fig. 1) to the detector:

$$A_{ij}(k, m) = \exp\left[-\int_{b_{ij}}^{\text{dector}} \mu(s_{km})ds_{km}\right], \qquad (3)$$

where b_{ij} is the entrance point to the pixel (i,j) and s_{km} is the length along the projection ray.

In the backprojection operation, the image value at pixel (i,j) is given by

$$x_{ij} = \sum_{k,m} W_{ij}(k, m)p_{km}. \qquad (4)$$

Here, the weighting factors represent the amount a projection bin will contribute to an image pixel for the backprojection operation. The attenuated projector-backprojector given in Eqs. (1) and (4) was used in the iterative reconstruction algorithms to model the attenuation of the emitted photons.
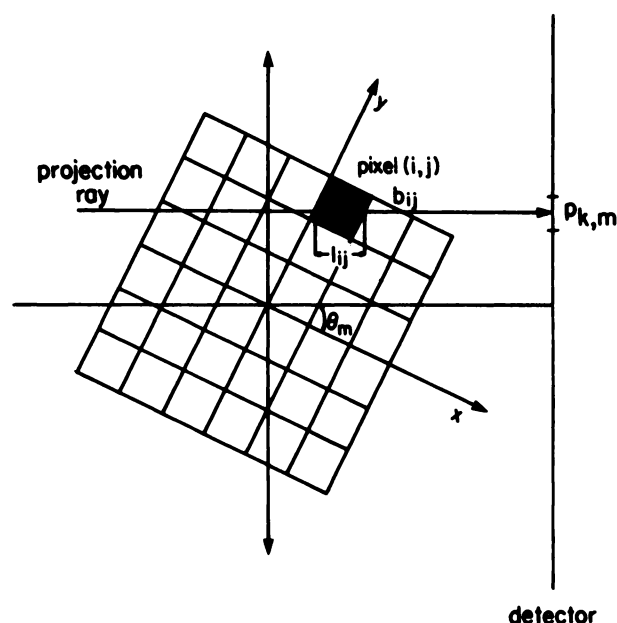

FIGURE 1
A typical projection ray at projection angle θ_m and bin k intersects the pixel (i,j) at the point b_{ij} nearest the detector. The length of the intersection is l_{ij}.

Iterative Chang Attenuation Correction Algorithm

The Chang algorithm (2) was initially implemented as a single step postprocessing technique to correct for attenuation of single photon emissions in SPECT imaging. After reconstruction of the attenuated data the value at a pixel is increased by a factor which is the reciprocal of the average of all attenuation factors $W_{ij}(k,m)$ over all projection angles, where $W_{ij}(k,m)$ is given in Eq. (2). This postprocessing technique was later implemented iteratively (3,4) by comparing at successive iterations the attenuated projections [Eq. (1)] of the result of the postprocessing with the measured data and iteratively adding to the previous estimate of the reconstruction, the reconstruction of the difference between the measured data and this result.

The iterative Chang algorithm can be stated mathematically by the following equation (n = −1, 0, 1, 2 · · ·)

$$x_{ij}^{n+1} = x_{ij}^n + \sum_{k,m} F_{ij}(k, m)\Delta^n q_{km} \Big/ \sum_{k',m'} W_{ij}(k', m') \quad (5)$$

where

$$\Delta^n q_{km} = \sum_{k'} c_{k-k'}(p_{k'm} - p_{k'm}^n), \quad (6)$$

$F_{ij}(k,m)$ is the weighting factors without attenuation, c_k is the discrete reconstruction convolver, and p_{km}^n at the nth iteration is the attenuated projection [Eq. (1)] of the estimated reconstruction at the nth iteration. For n = −1, it is assumed that $x_{ij}^n = 0$ and $p_{km}^n = 0$.

The one-step postprocessing correction x_{ij} will compensate exactly for attenuation if a point source is located within a uniform attenuator. The one step correction gives a fairly good approximation but not an exact solution if the source is distributed within a constant attenuator. For nonuniform attenuators like the chest region, the one-step correction will not correct for either a distributed source or a point source. After one or two iterations the iterative Chang algorithm gives a better solution but then tends to diverge and amplify statistical fluctuations with increasing iteration.

Iterative EM Attenuation Correction Algorithm

Historically, the maximum likelihood EM algorithm has been used with success in diverse applications (15). More recently, it has been applied in the reconstruction of both transmission and emission CT data (8,9). Unique in the approach taken in references (8) and (9), it takes into account the Poisson statistics of photon counting in modeling the noise properties in the image reconstruction process.

The iterative EM algorithm is a method which computes the maximum likelihood estimate (9,16). Each iteration of the EM algorithm consists of two steps. In the E-step, one forms the conditional expectation of the likelihood function. In the M-step, the conditional expectation is maximized with respect to the nth estimate of the reconstructed image to give the new (n+1)th estimate. The EM algorithm is given by (9)

$$x_{ij}^{n+1} = \frac{x_{ij}^n}{\sum_{k',m'} W_{ij}(k', m')} \sum_{k,m} \left[W_{ij}(k, m) \frac{p_{km}}{p_{km}^n} \right], \quad (7)$$

where the projection p_{km}^n is the attenuated projection of the nth estimate [Eq. (1)]. The summation in Eq. (7) over (k,m) is the attenuated backprojection operation [Eq. (4)].

Besides modeling the statistical noise accurately, the maximum likelihood method possesses other important properties. If the initial estimate of the reconstructed image is positive, the EM algorithm automatically sets a non-negativity constraint. Also, the expected number of total counts at each iteration remains constant.

METHODS

Determination of the Attenuation Coefficient Distribution

The attenuation coefficient distribution was determined by the transmission CT method. A schematic diagram of the transmission CT setup using a collimated sheet radiation source is shown in Figure 2. The sheet source was used to obtain the transmission projection data (17). In order to reduce radiation exposure to the patient and image degrading effects of scattered transmission photons, a special parallel hole collimator was used to restrict the direction of the emissions from the sheet source. The patient setup consisted of a collimated sheet source mounted opposite the camera on the rotating gantry of a GE 400 AC/T SPECT system. Using a thermoluminescent dosimeter, the measured radiation dose to the patient using 20 mCi of technetium-99m (^{99m}Tc) pertechnetate in the collimated sheet source and 20 min of exposure time was less than 1mR.

Phantom Study

In order to compare the different reconstruction methods, a phantom study was performed. As shown in Figure 3A, the phantom consisted of an elliptically-shaped cylindrical container which was used to simulate the body. The inside diameters of the major and minor axes of the elliptical phantom are 30.5 cm and 22 cm, respectively. A cardiac insert was placed inside the body phantom. The insert is made of two concentric chambers separated by 1.0 cm. The space between the concentric chambers can be filled with water containing radioactivity to simulate uptake in the myocardium.
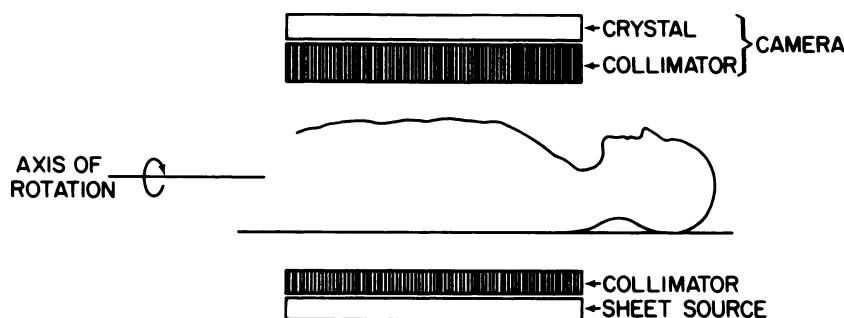

FIGURE 2
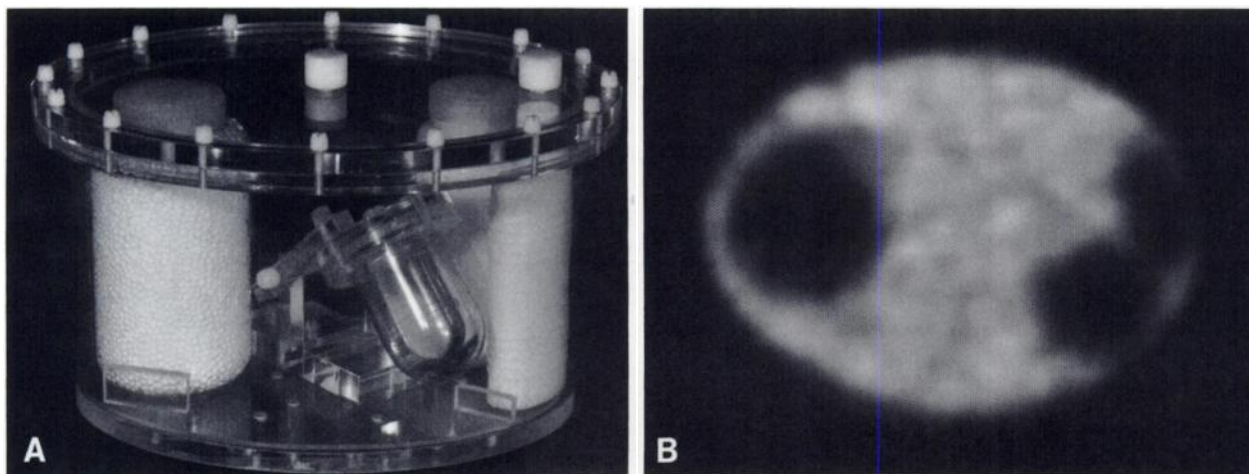Schematic diagram of the transmission CT setup using a collimated sheet source.

FIGURE 3
A: Cardiac phantom designed to simulate the myocardium inside the chest region with nonuniform attenuation coefficient distribution. B: Example of a transmission CT image of the cardiac phantom.

Three plastic bottles were placed inside the body phantom tightly surrounding the cardiac insert. The bottles were filled with a mixture of styrofoam beads and water to simulate the photon attenuation properties of the lung tissue. The attenuation coefficient of the mixture of styrofoam beads and water was about one-third that of water alone and a close approximation to that of the lung tissue.

Transmission projection data were collected in 64×64 matrices using the collimated sheet source with 12 mCi of ^{99m}Tc. A total of 64 views over 180° were acquired. At 20 sec/view, the average total counts per view were ~280,000 and the minimum transmitted count was ~10 with the incident count of ~190 per pixel. The incident flux was measured by collecting a static image of the uniform sheet source without the phantom. A measurement of 300 sec gave an average incident flux of ~1,500 counts per pixel.

Figure 3B shows a transmission CT image of the phantom at a level through the cardiac insert. The image intensity is proportional to the attenuation coefficient distribution in the cross sectional slice. The simulated lung is clearly separated from the surrounding water which is contained in the remainder of the cylindrical phantom.

The iterative EM algorithm was used to reconstruct the transaxial images of the attenuation coefficient distributions. The weighting factor used was the ray length within each pixel. The result after the 20th iteration was chosen for the reconstructed distribution. A three-dimensional smoothing filter (1, 2, 1) was then applied to the stack of transaxial images to obtain the final smoothed image set.

The attenuation coefficient distribution obtained with the ^{99m}Tc transmission sheet source was determined for the 140 keV photon energy. Whereas in the emission study, the counts were detected from three energy windows (60–88 keV, 122–149 keV, and 150–184 keV) placed over the three major energy peaks of ^{201}Tl which are 135 keV (2.7%/Disintegration), 167 keV (10%/Disintegration), and 68.9–80.3 keV with a mean at ~75 keV (94.4%/Disintegration). For these energies the total linear attenuation coefficient of photons in water varies from about 0.184/cm at 75 keV to 0.145/cm at 167 keV. In order to use the measured distribution of attenuation

coefficients in the emission reconstruction, the measured distribution of attenuation coefficients for ^{99m}Tc at 140 keV was scaled so that it would be equivalent to the emission energy of ^{201}Tl. Since the high energy emissions of ^{201}Tl are only a small fraction of the total emissions, the scaling of the distribution of linear attenuation coefficients assumed all photons of ^{201}Tl were 75 keV photons. It was also assumed that the linear attenuation coefficient varies linearly with energy between 75 keV and 140 keV. Based upon these assumptions, the estimated attenuation coefficient μ_{Tl} for the ^{201}Tl emissions was approximated from the measured attenuation coefficient μ_{Tc} for ^{99m}Tc using

$$\mu_{Tl} = \frac{\mu_{Tl}^{H_2O}}{\mu_{Tc}^{H_2O}} \mu_{Tc},\tag{8}$$

where $\mu_{Tl}^{H_2O} = 0.184$/cm and $\mu_{Tc}^{H_2O} = 0.153$/cm are the attenuation coefficients for water at the ^{201}Tl (75 keV) and ^{99m}Tc (140 keV) energies. This gives a ratio of $\mu_{Tl}^{H_2O}$ and $\mu_{Tc}^{H_2O}$ of ~1.2.

After the transmission CT study, a concentration of 1.9 μCi/ml was put in the myocardium and a concentration of 0.18 μCi/ml of ^{201}Tl chloride was put in the rest of the heart-lung phantom except for the lung chambers where nothing was injected. The phantom was then repositioned exactly as in the transmission CT study. The collimated sheet source was removed from its holder. To simulate the clinical situation, the emission projection data were summed over three energy windows, i.e., 67.5 to 82.5 keV, 121.5 to 148.5 keV and 150.3 to 183.7 keV and collected in 64×64 matrices in 64 views over 180°. The starting angle was 45° left posterior oblique with the camera rotating 180° right anterior oblique. At 20 sec/view, the average total counts per view were ~100,000.

The emission projection data were reconstructed using the filtered backprojection method and an iterative EM algorithm without attenuation correction. A ramp filter was used in the filtered backprojection algorithm. The same projection data were also reconstructed using the iterative Chang and the iterative EM algorithm with attenuation correction. The attenuation distribution information obtained from the trans-

mission CT image was used in the attenuation correction schemes.

To reduce image noise, a three-dimensional filter (0.3, 1, 0.3) was applied to the emission reconstructed images obtained from the different reconstruction methods. By using the same smoothing filter, we ensure that any differences in reconstructed image quality of each algorithm was not caused by the filter function used.

In order to evaluate the quantitative accuracy obtained from the different reconstruction methods, a count density profile was drawn through the reconstructed images at a representative level that included the cardiac insert. Since the thickness of and the radioactivity concentration in both sides of the myocardium were the same, the count densities at both sides of the myocardium should also be the same. The actual count density profiles obtained from the reconstructed images provided information on the quantitative accuracy of the reconstruction methods.

Patient Study

In a ^{201}Tl stress study, the patient was subjected to cycling exercise. At the peak of stress, a 2 mCi dose of ^{201}Tl chloride was injected intravenously and the exercise continued at the same level for 90 sec. Following this the patient was transferred to the SPECT system for the emission scan. The time lapse between the injection and the onset of the emission scan was less than 5 min. The emission projection data were acquired in 64 × 64 matrices. Data were summed over three energy windows, i.e., 67.5 to 82.5 keV, 121.5 to 148.5 keV, and 150.3 to 183.7 keV. The starting angle was 45° left posterior oblique with the camera rotating 180° right anterior oblique. A total of 64 views were collected. At 30 sec/view, the emission scan time was 32 min with an average of ~63,000 total counts per view.

After collection of the emission data, the collimated sheet source with 20 mCi of ^{99m}Tc was installed and the energy window reset to 20% over the 140 keV peak. Without moving
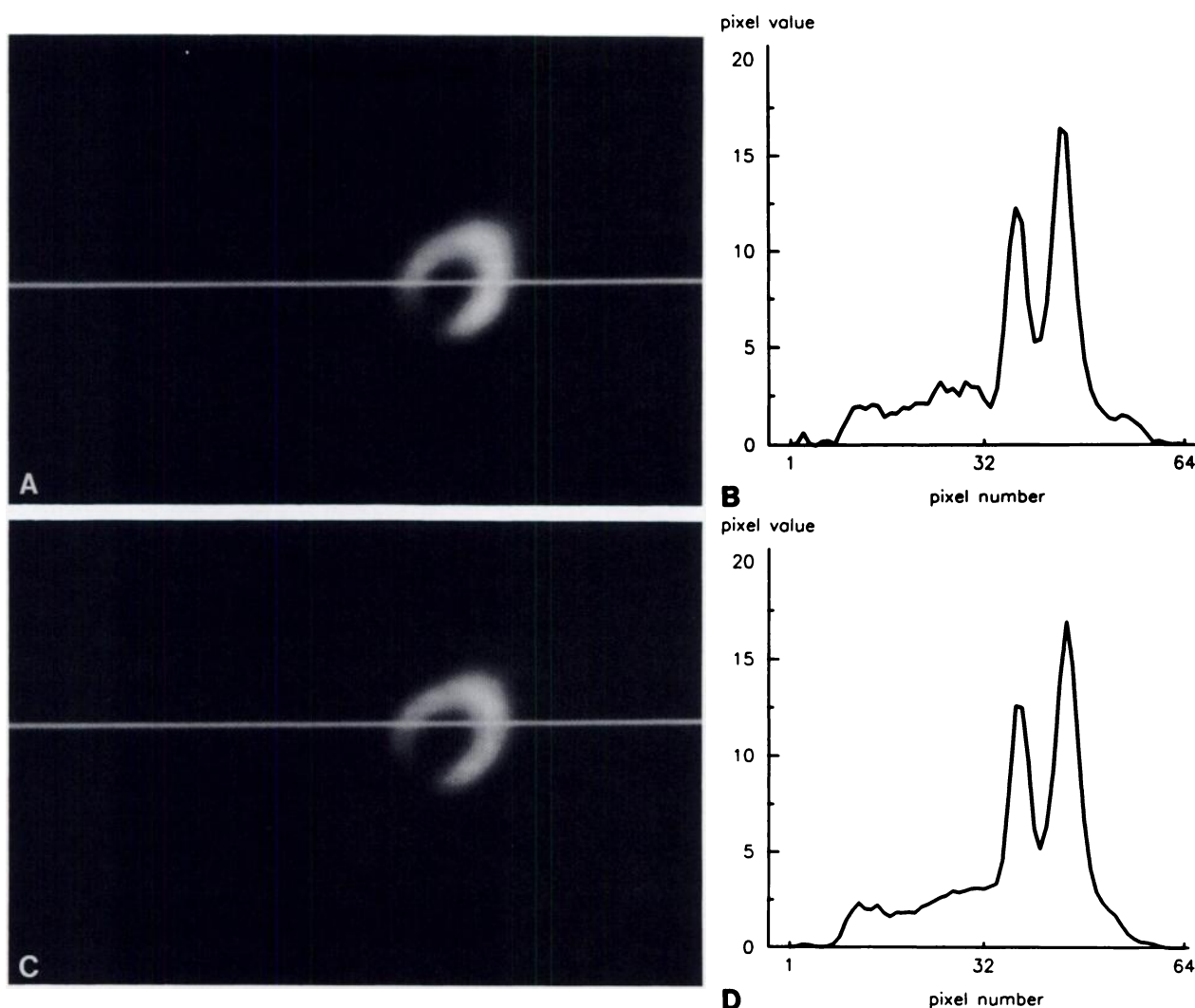

FIGURE 4

A: Emission CT image of the cardiac phantom obtained using the filtered backprojection algorithm without attenuation correction. The image slice is at the same location as that in Figure 3B. B: Profile through the myocardium as shown in A. C: Emission CT image of the cardiac phantom obtained from using the iterative EM algorithm without attenuation correction after the 30th iteration. The image slice is the same as that used in Figure 4A. D: Profile at the same level as that shown in Figure 4B.

the patient, the transmission projection data were acquired in 64 × 64 matrices and in 64 views over 180°. At 30 sec/view, the total transmission scan time was 32 min and the average total counts were ~225,000 per view. The minimum transmitted count per pixel was ~10 and the incident counts were 480 per pixel. After the patient was removed a static image of the uniform sheet source was collected for 120 sec. This gave an average count per pixel of ~1,700.

The same reconstruction and processing techniques used in the phantom study were applied to the patient data.

RESULTS

Phantom Study

Figure 4A shows the emission reconstructed image obtained from the filtered backprojection algorithm without attenuation correction. The slice is at the same location as the transmission CT slice in Figure 3B.

Figure 4B is a profile of the count density variations for the section drawn in Figure 4A.

Figure 4C shows for the same slice the emission reconstructed image obtained from the iterative EM algorithm without attenuation correction. It was found that the reconstructed image resolution improves with an increase in iteration but the image noise increases concurrently. The result after 30 iterations was chosen as an optimum solution that had good resolution with an acceptable noise level. Figures 4B and 4D show that the count density profiles from images obtained with the filtered backprojection and iterative EM algorithms are similar. In addition they both show a count density that is lower at the septum than at the lateral wall of the myocardium, although the radioactivity concentration is the same throughout the entire cardiac insert. The similarity in the profiles indicates that the iterative EM algorithm provides the same quantitative infor-
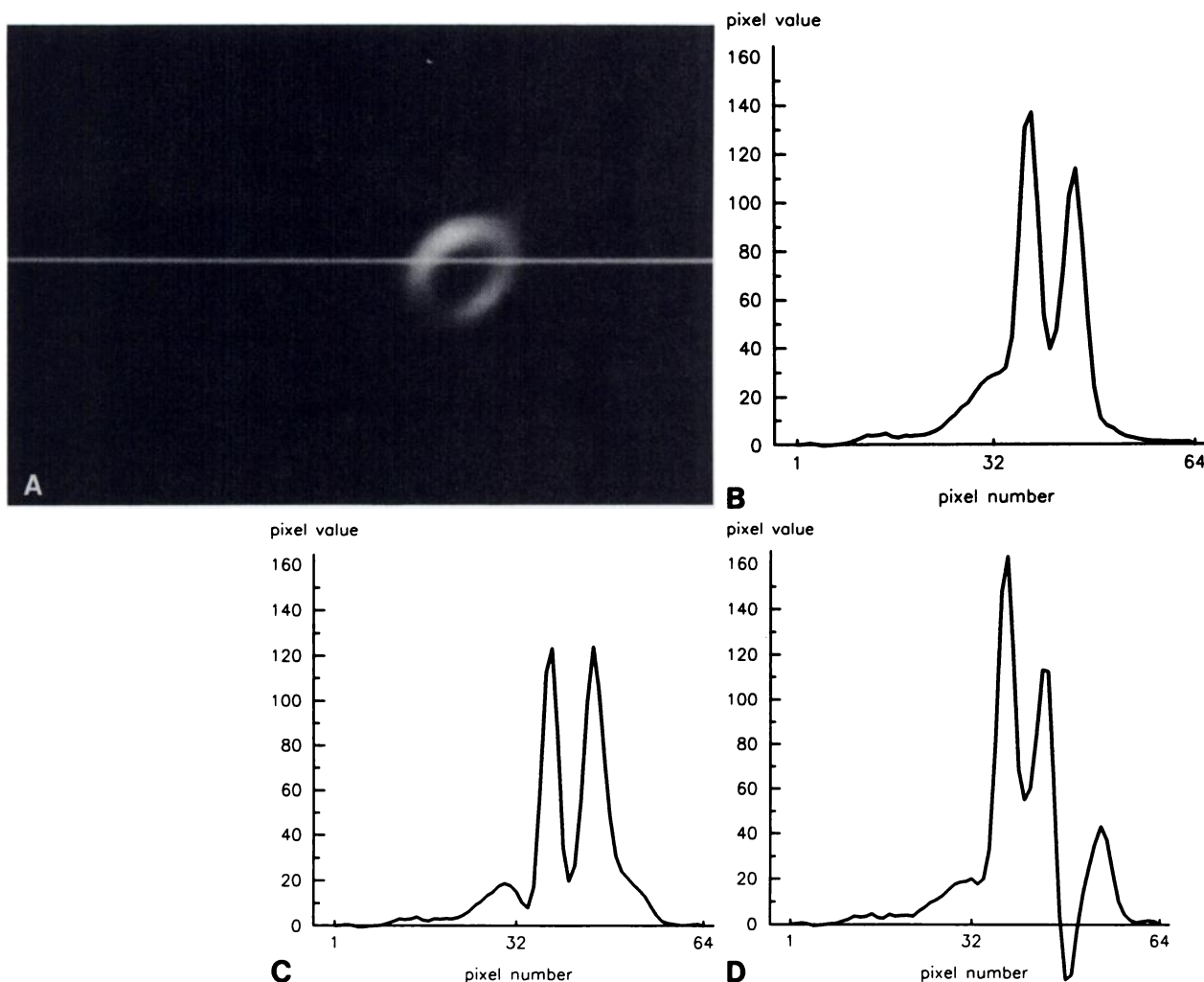

FIGURE 5
A: Emission CT image of the cardiac phantom obtained from using the iterative Chang algorithm with attenuation correction after the 1st iteration. The image slice is the same as that used in Figure 4. B: Profile at the same level as that shown in Figure 4. C: Profile after two iterations of the iterative Chang algorithm. D: Profile after 6 iterations of the iterative Chang algorithm.

mation as the filtered backprojection method if no attenuation correction is applied. However, the image quality appears to be better with the iterative EM algorithm in terms of improved image noise.

Figure 5A shows results after the 1st iteration of the iterative Chang algorithm with correction for nonuniform attenuation. The reconstructed image corresponds to the same slice and profile location as those in Figure 4. In Figure 5B, the profile has a greater magnitude than the filtered backprojection and iterative EM algorithms without attenuation correction. However, after one iteration the profile does not show equal count density in the septal and lateral walls of the myocardium. Figure 5 also shows profiles at the same location after two and six iterations. The profile has equal amplitudes in the septal and lateral walls after iteration two but then tends to diverge as the iteration increases. At iterations greater than eight the profiles become very distorted.

Figure 6A shows the emission reconstructed image obtained with the iterative EM algorithm after the 30th iteration with attenuation correction. The profile in Figure 6B was drawn at the same level as in Figure 4 and shows equal count density at the septal and lateral walls of the cardiac insert. Comparing Figures 6B and 5B we see that both profiles give equal amplitude in the septal and lateral walls but the iterative Chang algorithm gives a reconstructed slice profile of greater magnitude than the iterative EM algorithm. From the behavior of the iterative Chang algorithm for higher iterations, it is surmised that the EM algorithm with attenuation correction is potentially closer to the true slice profile.
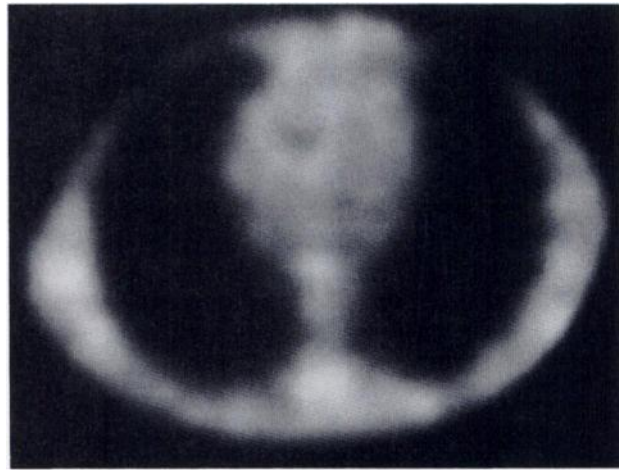

FIGURE 7
Transmission CT image of the patient.

Patient Study

The results of the ^{201}Tl stress study are shown in Figures 7 through 11. An example of the transmission CT image depicting the attenuation coefficient distribution is shown in Figure 7. Regions with different attenuation coefficients such as the muscle, lungs, and myocardium are demonstrated.

Figures 8 through 11 show emission CT images for the same slice using the various reconstruction methods. The attenuation coefficient distribution in Figure 7 was used in the iterative Chang and the iterative EM reconstruction algorithms for attenuation correction. Comparing the profiles, one can see that the iterative EM algorithm with correction for nonuniform atten-
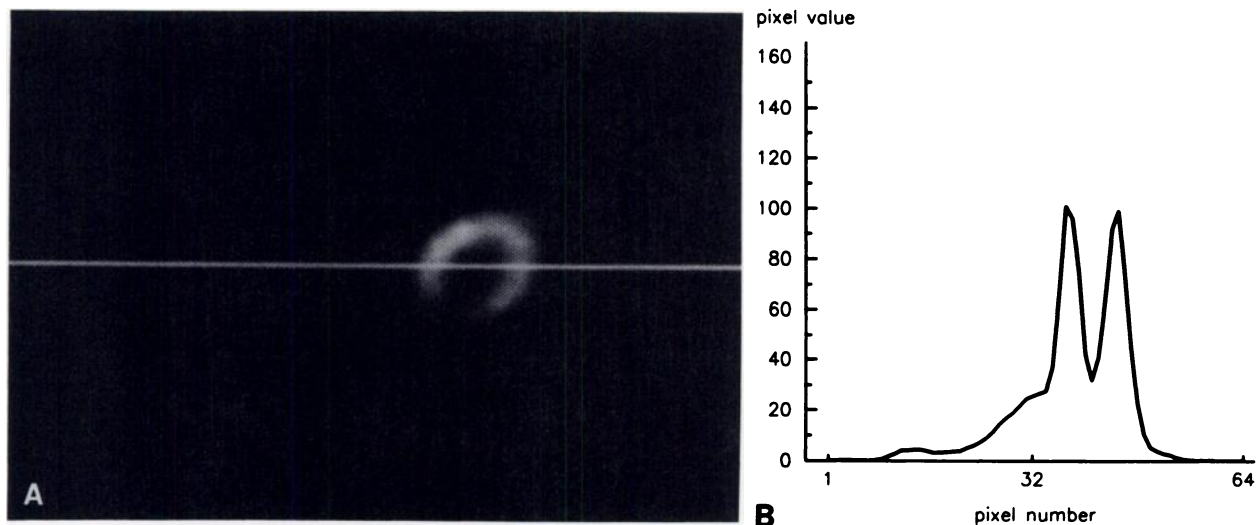

FIGURE 6
A: Emission CT image of the cardiac phantom obtained from using the iterative EM algorithm with attenuation correction after the 30th iteration. The image slice is the same as that used in Figure 4. B: Profile at the same level as that shown in Figure 4.
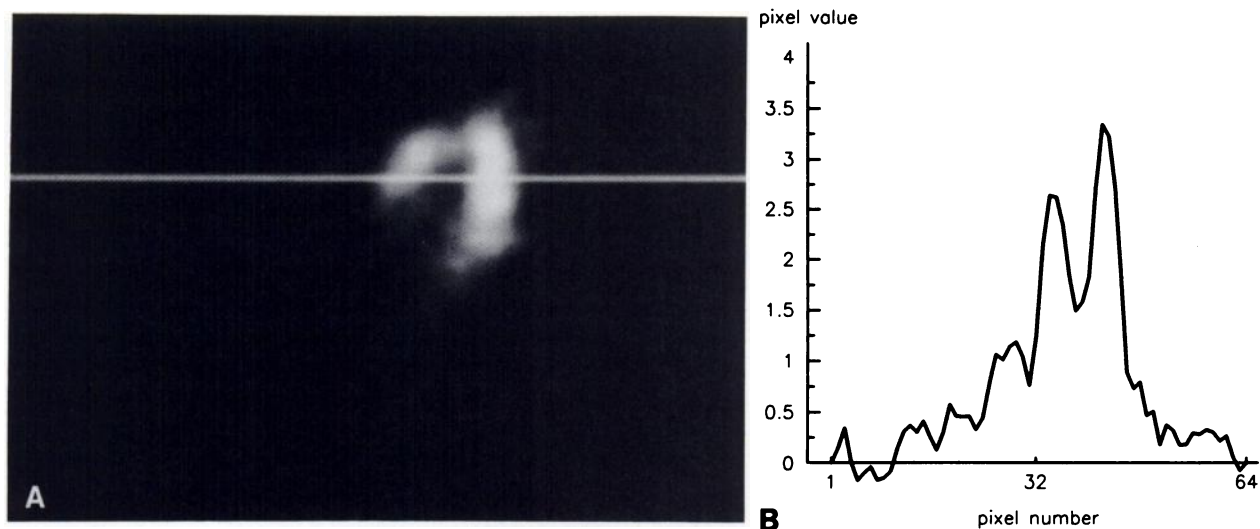
FIGURE 8
A: Emission CT image from the patient study using the filtered backprojection algorithm without attenuation correction. The image slice is the same as that used in Figure 7. B: Profile drawn the center of the myocardium as shown in A.

uation is the only method that gives nearly equal activity in the septal and left ventricular walls. Also, the results for the iterative EM algorithm have lower image noise fluctuations than those for the iterative Chang and the filtered backprojection algorithms.

Profiles at the same level for the patient shown in Figure 8 after two and six iterations of the Iterative Chang algorithm progressed as in the phantom study. The septal activity did not equal that of the lateral wall in any iteration.

DISCUSSION

This study verified that (a) better quantitation in cardiac SPECT is possible using iterative reconstruction algorithms and a transmission CT study to measure the nonuniform attenuation distribution, (b) the iterative EM algorithm with an attenuated projector-backprojector more accurately reconstructs the source distribution in the myocardium than the iterative Chang algorithm, and (c) the iterative EM algorithm gives better image quality in terms of less statistical noise, better spatial resolution, and reduction in image artifacts and distortions than the conventional filter backprojection algorithm. The patient and phantom studies demonstrated that the iterative EM algorithm with attenuation correction gives equal count densities in the septal and lateral walls of a normal myocardium. While, the iterative Chang algorithm does not give equal count densities where equal count densities are known to exist; it amplifies statistical noise; and it diverges with increasing iteration so that after as few as eight iterations the image becomes severely distorted.

The correction for attenuation in cardiac SPECT using ^{201}Tl can have significant clinical implications. First, attenuation correction increases the overall con-

centration by as much as 500% in the myocardium and offers significant improvement in the quantitative comparison over a large spectrum of patients including both men and women. In addition, since with attenuation correction equal count densities can be obtained in the septal and lateral walls of a normal myocardium, this information can be used as an important point of reference for diagnosing cardiac lesions. For example, it can be helpful in diagnosing large area, low contrast transmural defects in the septum where without attenuation correction it would be difficult to determine whether decreased counts in the septum is due to a defect or due to attenuation. Likewise, it can be useful in detecting diffused defects at the lateral wall where without attenuation correction it becomes difficult to determine at what contrast ratio between lateral wall and septum can one differentiate lesions from attenuation artifacts. Moreover, inadequate attenuation correction can result in significant distortion of shape that can create errors in quantitating myocardial infarcts.

There are some clinical implications of attenuation correction that are not as yet fully understood and require further research. It is not clear at this point whether attenuation correction improves or reduces septal lesion contrast. Present ROC studies on computer generated data seem to indicate that the detectability of small septal lesions are independent of attenuation correction. However, more phantom experiments are required to determine the lowest threshold for lesion size for which this remains true. Another aspect that warrants investigation is the observation that patients with elevated left hemidiaphragms may have low counts in the inferior wall. Women with large breasts may present a similar problem. For these cases, using the present doses of ^{201}Tl and standard collimators, it is possible that after attenuation correc-
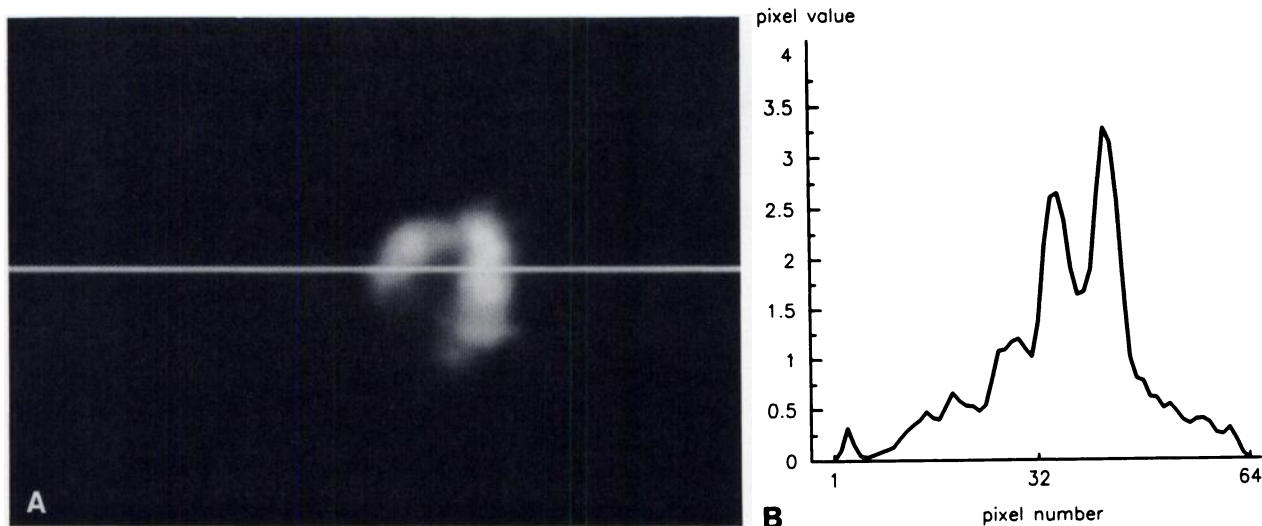
FIGURE 9
A: Emission CT image from the thallium patient study using the iterative EM algorithm without attenuation correction after the 30th iteration. The image slice is the same as that used in Figure 8. B: Profile at the same level as that shown in Figure 8.

tion errors will be so severe that the results will not yield sufficient contrast resolution. We know that at these low counts the statistical errors depend more strongly on the emission statistics than on the transmission statistics so that even increasing the transmission statistics will not improve the results (*1*).

The transmission tomographic study is primarily required to delineate the lung regions from the surrounding tissue. With present hardware this requires a separate study from the emission study and can require imaging times of more than an hour which is very uncomfortable for the patient. Methods have been investigated where transmission and emission data are collected simultaneously using dual energy acquisition mode. This is possible if the transmission and emission sources emit photons with different energies. For example, gadolinium-153 with photon emissions at 99 keV can be used in the transmission source with some of the new ^{99m}Tc heart radiopharmaceuticals being used as the emission radionuclide (*18*). However, scatter from the higher energy emission source contribute to the acquisition of the transmission data and will have to be compensated for if this method is to be successful.

Other image degrading effects in SPECT such as collimator-detector response, scatter, and heart motion
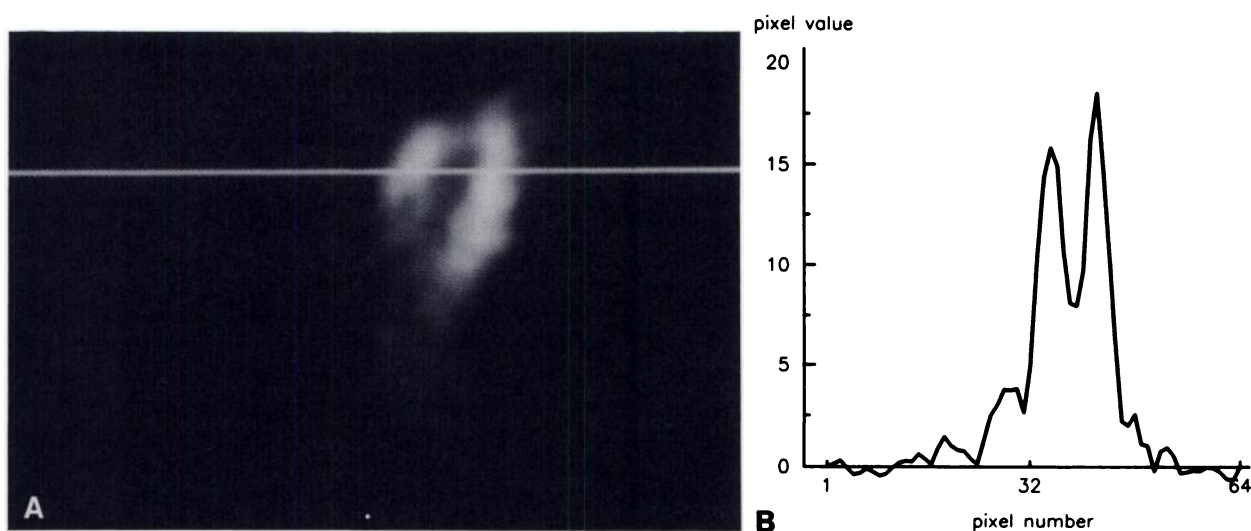

FIGURE 10
A: Emission CT image from the Tl patient study using the iterative Chang algorithm with attenuation correction after the 1st iteration. The image slice is the same as that used in Figure 8. B: Profile at the same level as that shown in Figure 8.
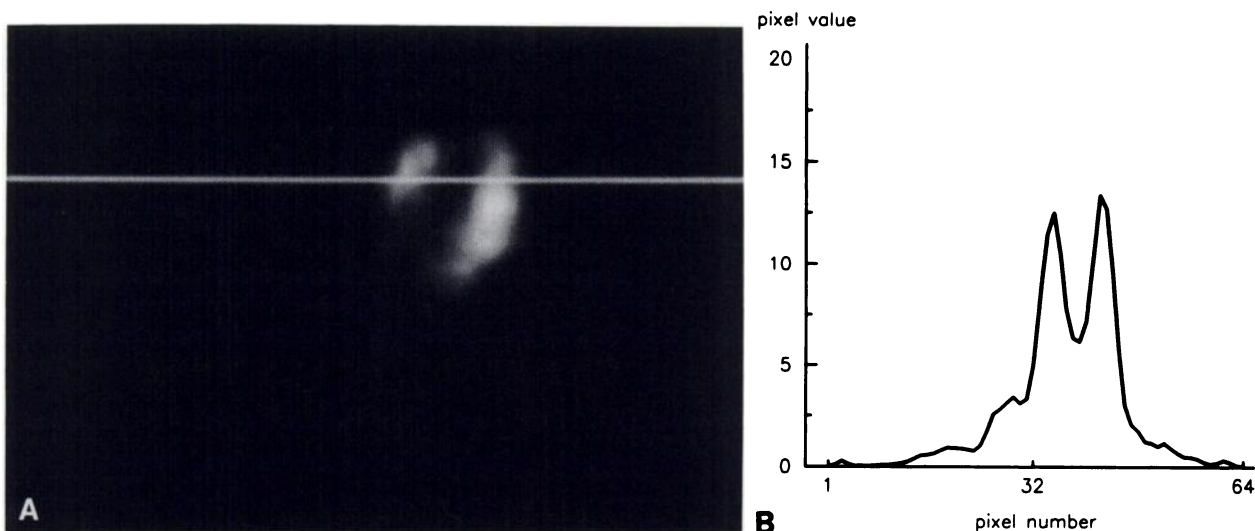
FIGURE 11

A: Emission CT image from the patient study using the iterative EM algorithm with attenuation correction after the 30th iteration. The image slice is the same as that used in Figure 8. B: Profile at the same level as that shown in Figure 8.

have not been compensated for in the present study. The maximum likelihood method includes the stochastic information of the detection model and can be extended to include the effects of detector response and scatter (*19*). Also, the ^{201}Tl SPECT study described in this paper was ungated due to the limited count density and the acquired data were averaged over many cardiac cycles. The ungated results can cause a blurring of the myocardium. Accurate measurement of wall thickness may require cardiac gating.

The iterative EM algorithm converges slowly and requires many repetitive calculations and lengthy processing time. Recently, acceleration methods have been proposed to reduce the computational requirements of the EM algorithm (*20–24*). We have found that implementation of the algorithm in a small array processor substantially increases the processing speed. Further increase in computational speed may be achieved through the use of faster and more powerful array processors. An alternative approach would be the implementation of algorithms in specially designed "hard-wired" processors.

ACKNOWLEDGMENT

REFERENCES

1. Gullberg GT. The attenuated Radon transform: theory and application in medicine and biology. PhD. Dissertation, University of California at Berkeley, 1979.
2. Chang LT. A method for attenuation correction in radionuclide computed tomography. *IEEE Trans Nucl Sci* 1978; NS-25:638–643.
3. Manglos SH, Jaszczak RJ, Floyd CE, Hahn LJ, Greer KL, Coleman RE. Non-isotropic attenuation in SPECT: phantom tests of quantitative effects and compensation techniques. *J Nucl Med* 1987; 28:1584–1591.
4. Manglos SH, Jaszczak RJ, Floyd CE. Weighted backprojection implemented with a non-uniform attenuation map for improved SPECT quantitation. *IEEE Trans Nucl Sci* 1988; NS-35:625–628.
5. Gullberg GT, Huesman RH, Malko JA, Pelc NJ, Budinger TF. An attenuated projector-backprojector for iterative SPECT reconstruction. *Phys Med Biol* 1986; 30:799–816.
6. Gordon R, Bender R, Herman GT. Algebraic reconstruction techniques (ART) for three-dimensional electron microscopy and x-ray photography. *J Theor Biol* 1970; 29:471–481.
7. Huesman RH, Gullberg GT, Greenberg WL, Budinger TF. User Manual, Donner Algorithms for reconstruction tomography, Lawrence Berkeley Laboratory, University of California, 1977.
8. Shepp LA, Vardi Y. Maximum likelihood reconstruction for emission tomography. *IEEE Trans Med Imag* 1982; MI-1:113–122.
9. Lang K, Carson R. EM reconstruction algorithms for emission and transmission tomography. *J Comp Assist Tomogr* 1984; 8:306–316.
10. Frieden BR. Restoring with maximum likelihood and maximum entropy. *J Opt Soc Am* 1972; 62:511–518.
11. Minerbo G. MENT: a maximum entropy algorithm for reconstructing a source from projection data. *Comput Graph Image Process* 1979; 10:48–68.
12. Gullberg GT. Entropy and transverse section reconstruction. In: Raynaud C, Todd-Pokropek A, eds. *Information processing in scintigraphy*. Proceedings of the IVth International Conference, Orsay, France, 1975: 325–332.
13. Budinger TF, Cahoon JL, Derenzo SE, Gullberg GT,

Moyer BR, Yano Y. Three dimensional imaging of the myocardium with radionuclides. *Radiology* 1977; 125:433–439.

14. Malko JA, Van Heertum RL, Gullberg GT, Kowalsky WP. SPECT liver imaging using an iterative attenuation correction algorithm and an external flood source. *J Nucl Med* 1986; 27:701–705.
15. Rao CR. Linear statistical inference and its applications. New York: Wiley and Sons, 2nd Ed., 1973.
16. Dempster AP, Laird NM, Rubin DB. Maximum likelihood from incomplete data via the EM algorithm. *J R Stat Soc Series* B, 1977; 39:1–38.
17. Maeda H, Itoh H, Ishii Y, Mukai T, Todo G, Fujita T, Torizuka K. Determination of the pleural edge by gamma-ray transmission computed tomography. *J Nucl Med* 1981; 22:815–817.
18. Bailey DL, Hutton BR, Walker PJ. Improved SPECT using simultaneous emission and transmission tomography. *J Nucl Med* 1987; 28:844–851.
19. Tsui BMW, Hu H-B, Gilland DR, Gullberg GT. Implementation of simultaneous attenuation and detector response correction in SPECT. *IEEE Trans Nucl Sci* 1988; NS-35:778–783.
20. Politte DG. Reconstruction algorithms for time-of-flight assisted positron emission tomographs. MS thesis, Washington University, St. Louis, 1983.
21. Lewitt RM, Muehllehner G. Accelerated iterative reconstruction for positron emission tomography based on the EM algorithm for maximum likelihood estimation. *IEEE Trans Med Imag* 1986; MI-5:16–22.
22. Kaufman L. Implementing and accelerating the EM algorithm for positron emission tomography. *IEEE Trans Med Imag* 1987; MI-6:37–51.
23. Tanaka E. A fast reconstruction algorithm for stationary positron emission tomography based on a modified EM algorithm. *IEEE Trans Med Imag* 1987; MI-6:98–105.
24. Metz CE, Chen CT. On the acceleration of maximum likelihood algorithms. *SPIE Med Imag II* 1988; 914:344–349.